Method for Automatization of the Alignment of a Laboratory based X-ray Phase Contrast Edge Illumination System

T. P. Millard,[1, a)] M. Endrizzi,[1] K. Ignatyev,[2, b)] C. K. Hagen,[1] P. R. T. Munro,[3, 4] R. D. Speller,[1] and A. Olivo[1, c)]

[1)] *Department of Medical Physics and Bioengineering, University College London, Malet Place, Gower Street, London WC1E 6BT, UK*

[2)] *Diamond Light Source Ltd, Diamond House, Harwell Science and Innovation Campus, Didcot, Oxfordshire, OX11 0DE, UK*

[3)] *Optical+Biomedical Engineering Laboratory, School of Electrical, Electronic and Computer Engineering, The University of Western Australia, 35 Stirling Highway, Crawley, Western Australia 6009, Australia*

[4)] *Centre for Microscopy, Characterisation and Analysis, The University of Western Australia, 35 Stirling Highway, Crawley, Western Australia 6009, Australia*

(Dated: 21 August 2013)

Here we present a general alignment algorithm for an edge illumination x-ray phase contrast imaging system, which is used with the laboratory systems developed at UCL. It has the flexibility to be used with all current mask designs, and could also be applied to future synchrotron based systems. The algorithm has proved to be robust experimentally, and can be used for the automatization of future commercial systems through automatic alignment and alignment correction.

I. INTRODUCTION

X-ray phase contrast imaging (XPCi) has the potential to transform radiography as it obtains information about a sample by sensing sample induced phase changes to the x-ray wavefront. Information unavailable in an absorption based x-ray image is therefore gained, allowing for a more detailed study of a sample's structure.[1] As well as this extra information, XPCi can also give increased image contrast, and has the potential to allow for imaging at higher energies and thus lower dose.[2]

This form of x-ray imaging was first developed at synchrotrons using highly coherent synchrotron radiation.[3–5] These first methods generally require an x-ray source with high spatial coherence making it difficult to implement in a laboratory using conventional x-ray equipment. Some success has been had using these methods with microfocal sources,[1,6] and crystal based methods have been implemented using conventional sources.[7,8] In both cases low usable flux increases exposure times limiting the potential for the application of these approaches.

Interferometric methods based on gratings have also been developed at synchrotrons,[9–12] and then translated to conventional laboratory x-ray sources.[13] With a spatially coherent x-ray source two gratings with a pitch typically of a few microns are used. The second grating is placed at a Talbot distance away from the first, with a detector placed beyond the second grating to sense the interference pattern. The introduction of a sample distorts the projection of the self image of the first grating on to the second grating thus changing the detected signal. By scanning one grating with respect to the other,

a)Electronic mail: t.millard@ucl.ac.uk
b)Electronic mail: konstantin.ignatyev@diamond.ac.uk
c)Electronic mail: a.olivo@ucl.ac.uk

distortions in the signal caused by the sample can be analyzed to allow the extraction of phase, absorption and dark field images.

For this method to be used with conventional sources a third grating is added directly after the x-ray source switching the configuration from Talbot to Talbot-Lau.[13] This extra grating apertures the source to provide the required spatial coherence. An extra grating has the undesired effect of reducing the flux available for imaging, and the small grating pitch means that system stability is important. Both of these factors add complications when translating such a design to a practical environment.

The edge illumination system design discussed here is non-interferometric as it uses gratings with a pitch more than one order of magnitude larger than that used for the interferometric methods. This means that a grating in an edge illumination system splits an x-ray beam into independent non-interfering secondary beams. To avoid confusion with interferometric methods the gratings used for this system will be referred to as masks.

The edge illumination method was first developed at synchrotrons in the late 1990s,[14] and has more recently been translated to a laboratory environment.[15] The principle of the method is that a narrow beam of x-ray radiation is aligned so that it overlaps the edge of an x-ray sensitive region, such as a detector pixel. Distortions of the x-ray wavefront by a sample will change the detected intensity by deviating this beam either towards or away from the x-ray sensitive region. By creating an array of beams and an array of edges using masks the method can be extended to give phase sensitivity over a two dimensional pixelated detector. This method has been shown to work using sources with focal spots up to 100 μm,[16] and with tube voltages up to 100 kVp.[17,18] Here edge illumination is used to refer to the method in both its synchrotron and laboratory (coded-aperture) implementation.
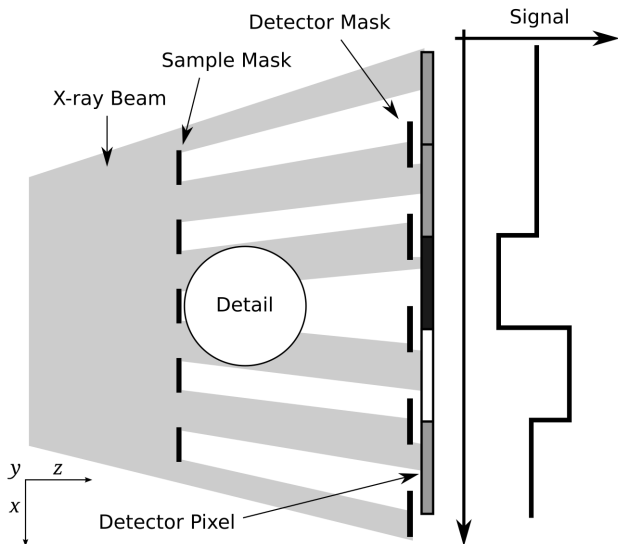
FIG. 1. Diagram depicting the basic principle of an edge illumination XPCi system. The secondary beams created by the sample mask undergo a shift when passing through the detail causing their movement on to or off of the detector mask generating contrast.

A diagram depicting the edge illumination method is shown in Fig. 1. The edge illumination system is aligned when the projection of both masks onto the detector forms a pattern with two-dimensional periodicity with period equal to the detector pixel dimension. The detector mask is positioned so that the transmission slits illuminate the central strip of every pixel, allowing for the most sensitive region of the detector pixel to be used for imaging.

To perform different imaging modes, images are taken with the sample mask illuminating different parts of the detector mask by translating it along the x axis. For phase retrieval two images are taken, with the sample mask illuminating, symmetrically, both edges of the detector mask apertures. An algorithm is then used to extract the phase and absorption images.[19]

The current system design is sensitive to phase gradients in one direction only, as the transmitting slits are all orientated in one direction. It would, however, be possible to design a system sensitive in two directions.[20,21] For any mask design the slits need to be finely aligned over the whole detector area to produce high quality images. The alignment procedure described here is particular to masks sensitive in one direction, though it could be trivially extended to masks sensitive in two directions.

II. OVERVIEW OF AN EDGE ILLUMINATION SYSTEM

There are currently two functional prototype laboratory based edge illumination systems at UCL. Both use commercially available detectors; a Hamamatsu
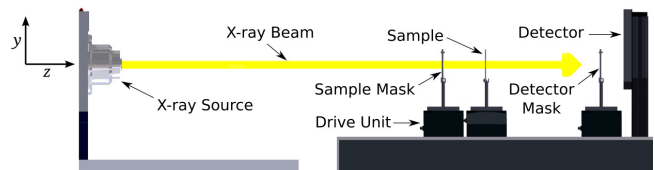

FIG. 2. Simple diagram of a laboratory Edge Illumination XPCi system in profile.

C9732DK flat panel detector with a pixel size of 50 μm, and an Anrad SMAM with 85 μm pixels. These systems also both use commercially available x-ray sources. An X-tek rotary target Tungsten source which has been used in hospital work since the 1980s,[22] with a focal spot size of approximately 50 μm,[23] and a Rigaku MicroMax 007 HF with a focal spot size of approximately 75 μm full width half maximum. Masks have been made to the authors design by Creatv MicroTech Inc. (Potomac, MD, USA) who electroplated gold on to a graphite substrate. The gold forms the absorbing parts of the mask, with the spaces in between being the transmitting slits. Both systems have a field of view of 60 × 60 mm, but much larger masks could be manufactured.

Masks used for the system have to be matched to the detector, as their pitch needs to fit the pitch of the detector pixels. For example a current system design using the Anrad SMAM detector has a sample mask with a pitch of 66.8 μm, and a detector mask with a pitch of 83.5 μm. This gives a source to sample mask distance of approximately 1.67 m, a sample mask to detector mask distance of approximately 0.37 m with a total system length of approximately 2 m (although the entire system could be scaled up or down proportionally). Current work is aimed at determining how much the total length of a system can be reduced whilst preserving sensitivity, as it has been anticipated that a system significantly smaller than 2 m can be designed.[16]

The detector mask has been designed so that there is a gap between it and the detector to leave space for the detector mask drive unit. In a commercial system the detector mask could be incorporated into the detector, reducing system complexity and leaving only one mask for alignment. A diagram of a typical system is shown in Fig. 2.

Two different mask designs have been used so far. One design creates a secondary beam of radiation for every pixel column, whereas the other creates a secondary beam for every other pixel column. These designs have been called non-column-skipping and column-skipping respectively. As has been previously reported, a column-skipping design is useful when employing a detector such as the Hamamatsu C9732DK which has a relatively high pixel spill out.[23] High pixel spill out results in contrast reduction and/or artifacts which a column-skipping mask design reduces. Figure 3 illustrates these two different mask designs, and shows the image seen on the detector when these masks are aligned and illuminated.
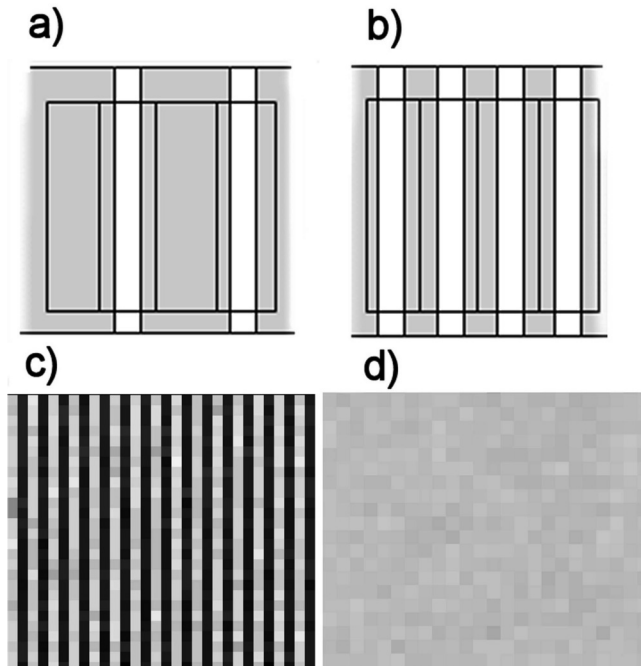
FIG. 3. Figures a and b illustrate two potential mask designs, with a being column-skipping and b being non-column-skipping. Figures c and d show the respective image as seen by the detector following alignment.
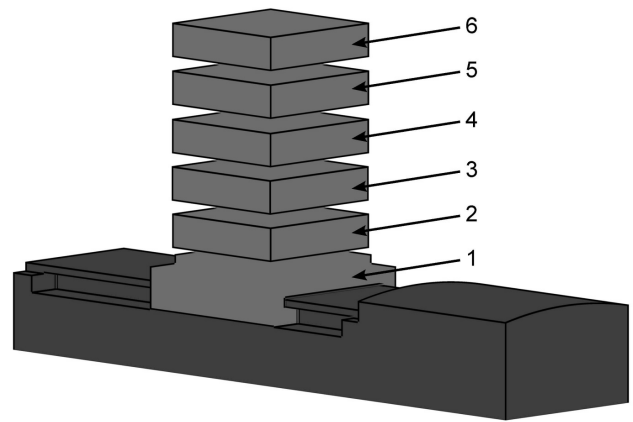

FIG. 4. Diagram of the drive unit used for mask positioning. 1 for translation along x axis. 2 for translation along y axis. 3 for translation along z axis. 4 for rotation about z axis. 5 for rotation about x axis. 6 for rotation about y axis.

III. MATERIALS AND METHODS

Masks are mounted on a drive unit consisting of a serial sequence of six motors as shown in Fig. 4, giving complete control over the orientation and position of each mask within the motors' range of operation. The detector could also be mounted on a drive unit, but in practice this is not necessary as it can be mounted first with the two masks then aligned relative to it.

A drive unit consists, in sequential order, of the following (1-6 in Fig. 4). A Newport M-ILS150 translation stage for translation along the x axis with a precision of 0.1 μm. A Newport MFA-CC with minimum incremental motion of 0.1 μm for translation along the z axis. A Newport M-VP-5ZA for translation along the y axis. Kohzu SA04B-RT and SA04B-RM cradles with a resolution of approximately $0.0014°$ for rotation about the x and z axes, and a Newport SR50 rotation stage with $0.001°$ resolution for rotation about the y axis. Motors are controlled using the appropriate controllers, a Newport XPS controller and Kohzu SC-400 controller. These interface with Experimental Physics and Industrial Control System (EPICS) which can be controlled either manually through a custom designed GUI, or using in-house IDL software. All data acquisition, processing and figure plotting are performed using the IDL software.

For alignment of interferometric systems in both optical and x-ray regimes, various methods based on the analysis of Moiré patterns are used. A Moiré pattern is generated when two gratings with slightly different period or rotation relative to each other are overlaid.

Using Moiré fringes is also an option for aligning an edge illumination system, but to generate the necessary mismatch in the projected period to obtain these patterns the masks have to be moved far out of alignment. This means that the Moiré fringes are not a true measure of system alignment, but instead a measure of system

Use of a non-column-skipping mask has a significant advantage over the use of a column-skipping mask as it gives a two times increase in available flux and spatial resolution in the non-scanning case. A non-column-skipping design has been implemented using the Anrad SMAM detector, which has a pixel spill out of approximately 5% horizontally meaning that artifacts from pixel spill out are less of a problem.

For production of the highest possible image quality both masks need to be aligned with respect to the source and detector to the point at which possible mask defects limit any improvement in alignment. A commercial design cannot require manual adjustment for minor alignment correction: the system alignment algorithm should be completely autonomous whilst having a degree of flexibility to allow for alignment of both the column-skipping and non-column-skipping mask designs. The algorithm presented in this paper could be incorporated in a commercial device to provide exactly that functionality.[24]

Potential mask defects can arise during mask manufacture. In general, potential defects can be divided into two categories: uneven deposition of absorbing material (in this case gold) to form the solid parts of the mask, and variation in slit width, again due to the deposition process. Preliminary investigations based on the effects these defects have on image quality show that variation in slit width is less than 1 μm, and that gold thickness varies by approximately $5\mu m$.
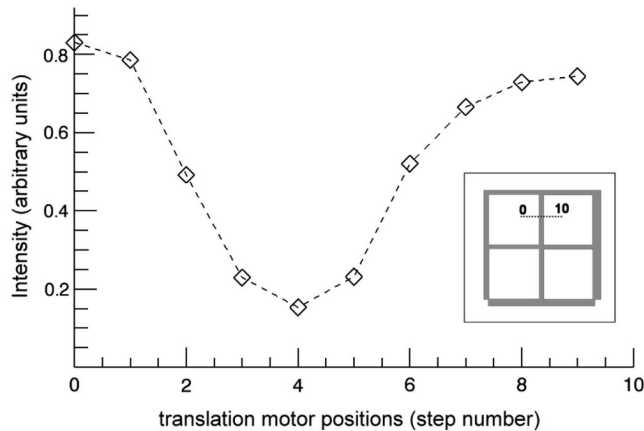
FIG. 5. Intensity detected in a single pixel when an aligned mask is scanned in the transverse x-direction in sub-pixel increments over the pixel edge.

misalignment whose validity is limited to the current z-position. Large mask translations needed to generate the Moiré patterns also make this impractical for a commercial system, as such a system would have limited space. A different strategy was therefore followed.

An ideal x-ray detector would have a uniform and homogeneous response function, although generally this is not the case. For example, flat panel detectors such as a direct conversion Selenium detector have an active volume consisting of a homogeneous layer of semiconductor material, and a periodic electrode structure which collects the electrons generated in the active area as a result of x-ray photon interaction with the semiconductor. Due to manufacturing constraints, the electric field in the active area generated by the electrodes is non-uniform, and typically decreased from the position in the pixel corresponding to the center of the electrode towards the edge of the pixel. As a result, the electron collection efficiency is non-uniform.[25,26]

This means that if a secondary beam is scanned transversely in the x-direction across the detector, the output will vary in a periodic manner related to the detector response. So the translation of an aligned mask in the x direction will effectively sample the detector point spread function, allowing visualization of the detector response at the sub-pixel level. Figure 5 illustrates an example of recorded intensity for one pixel as a function of translational increments (numbered 1 to 10). The minimum represents the position where the mask aperture traverses the pixel edge and is clearly visible on the plot. This physical effect can be used to devise an alignment algorithm.

IV. MASK ALIGNMENT PRINCIPLES

To first approximation, assuming a point source and (100% efficient) and homogeneous mask, the intensity of the beam incident on the detector plane ($I(x, y)$) can be written as shown in Eq. 1, with the (x, y) coordinate system lying on the plane of the detector.

$$I(x, y) = T(x, y) \times I_0(x, y) \tag{1}$$

$I_0(x, y)$ is the intensity of the incident beam in the absence of masks and $T(x, y)$ is the transmission function representing the mask geometry, both projected onto the detector plane. The transmission function of the mask can be written as

$$T(x, y) = \begin{cases} 1 \text{ if } \cos(\frac{2\pi x}{Mp}) \geq \cos(\frac{\pi w}{p}) \\ 0, \text{ otherwise} \end{cases} \tag{2}$$

Where p is the period of the mask and w is the aperture width. M is the magnification factor calculated using Eq. 3, where Z_{sm} is the source to mask distance and Z_{md} is the mask to detector distance.

$$M = \frac{Z_{md} + Z_{sm}}{Z_{sm}} \tag{3}$$

The signal recorded by a detector pixel is the product of the incident x-ray beam $I(x, y)$ with the geometrical detector pixel response function $R_{pix}(x, y)$, where $R_{pix}(x, y)$ takes arguments $x \leq |\frac{Mp}{2}|$ and $y \leq |\frac{Mp}{2}|$. This can be expanded for an array of uniform pixels as shown in Eq. 4, where n and m are integers and S_x and S_y is the pixel pitch in the two directions.

$$R_{det}(x, y) = R_{pix}(x + nS_x, y + mS_y) \tag{4}$$

A detector generally does not have a matrix of uniform pixels, due to individual pixel non-uniformity. However flat field correction of experimental data can compensate for both detector and beam non-uniformities, meaning that in practice we can assume a uniform response.

Images are taken by scanning a mask in sub-pixel steps (Δx) across the detector. The periodic response of the detector (Eq. 4) is modulated by the periodic incident beam (Eq. 1).

$$g(x, y; \Delta x) = I(x + \Delta x, y) \times R_{det}(x, y) \tag{5}$$

The position Δx for which the minimum intensity is detected for each pixel is then found, as shown in Eq. 6.

$$G(x, y) = \min_{\Delta x} g(x, y; \Delta x) \tag{6}$$

The phase mismatch between the periods of the beam incident on the detector (Eq. 1) and detector response function (Eq. 4) is an indication of mask misalignment. If $G(x, y)$ is constant then there is no phase mismatch and the alignment condition is satisfied, otherwise motor correction is required.

An aligned mask is in the correct position on the z axis, and has the correct rotation about the x, y and z axes. Translation on the x and y axes does not affect mask alignment. The y axis needs to be adjusted only so that the mask is in the correct position relative to the detector, and x axis translation is used to adjust the illumination level with the sample mask or the position of the detector mask slits over the detector. As a result there are four degrees of freedom that need to be optimized for a single mask.

The translation increment size determines the resolution of the system alignment and is limited by the precision of the x translation stage. Current equipment has a resolution better than one micron, which means that the position of the slit centerline projected onto the detector can be found with one micron accuracy, even though the detector pixel size is typically of several tens of microns. It is possible to align a mask to the point where mask defects prevent any further improvement in alignment, even if a step size finer than one micron is used. Moreover, this method could be used for the characterization of these mask defects which limit further improvement in alignment.

Since the sub-pixel detector response variation is a weak effect, to maximize the useful signal, the detector output is averaged using a moving window over the (x, y) plane. This gives an increased signal-to-noise ratio, but does not affect the alignment resolution as this is determined by the translation increment size. A 25 x 25 pixel window is used as this was found empirically to provide a balance between increased signal to noise and smoothing of higher frequency steps in G. The averaged signal from each pixel is recorded for each step of the scan, and then used to generate the plots shown in Fig. 6.

A. Tolerances

As discussed previously a mask is aligned when its projected pitch matches the pitch of the detector. Tolerances required for system alignment depend strongly on the system geometry. The effect of magnification means that a system will always be far less sensitive to misalignment along the z axis and rotation about the x and y axes, than rotation about the z axis. The following minimum motor step sizes are used regularly for alignment of the Anrad SMAM based system discussed previously. Distance along z of 50 μm, rotation about x and y axes of 0.1°, and 0.0025° about the z axis.

To calculate tolerances for mask alignment it first needs to be known at which point mask misalignment along the z axis causes steps to appear in the plot of G.

This was calculated using a model of mask alignment implemented in MATLAB, based on Eqs. 1-6 in this paper, in which Z_{sm} in Eq. 3 was modified to $Z_{sm} \pm \Delta z$. Δz was then increased or decreased from zero until the first step appeared in the simulated plot of G.

Rotation about the x axis (θ_x) moves the top and bottom of mask towards or away from the detector, whilst rotation about the y axis (θ_y) moves the sides of the mask towards or away from the detector. So the calculated Δz at which steps first appear can be used to find the tolerance of both θ_x and θ_y:

$$\Delta\theta_x = \pm \arcsin\left(\frac{2\Delta z}{nP_m}\right) \tag{7}$$

$$\Delta\theta_y = \pm \arcsin\left(\frac{2\Delta z}{nP_m}\right) \tag{8}$$

Misalignment of rotation about the z axis does not affect the distance of the mask along z; instead, at small angles of misalignment, it effectively shifts the mask period at the top and bottom of the mask relative to the middle. The tolerance at which one step will appear for θ_z can be calculated as shown in Eq. 9:

$$\Delta\theta_z = \pm \left[\arctan\left(\frac{nP_m + s}{nP_m}\right) - 45°\right] \tag{9}$$

The results of these calculations show that, for the sample mask of this system, assuming defect free masks, the plot of G will appear flat with a 2 μm x translation step so long as the mask is within the following range of its optimal position: distance along z of ± 27 μm, rotation about x and y axes of $\pm 0.066°$, and $\pm 0.0012°$ about the z axis. These values are in the same range as the minimum experimental motor step size. It should be noted that smaller step sizes could be used experimentally, as those used are less than the motors precision, but that smaller step sizes give no improvement in alignment due to mask imperfections.

V. MASK ALIGNMENT PROCEDURE

The procedure described works for both column-skipping and non-column-skipping masks; to use column-skipping masks, signal from every other pixel column is simply discarded.

A. Alignment of a single mask

To align a single mask it is first mounted on the drive unit in a position where the projected pitch is calculated to match the detector pixel pitch. The drive unit is placed in such a way that mask position and orientation can be optimized around this initial position.
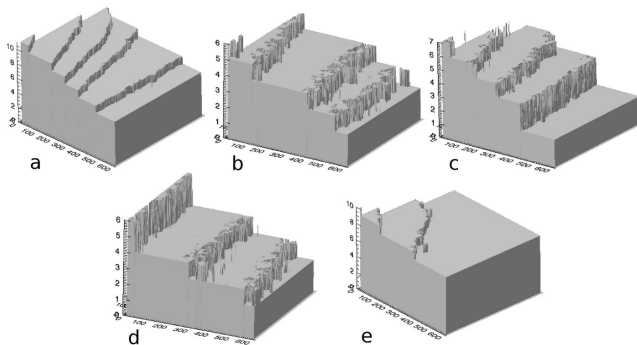
FIG. 6. Example plots of the function G showing the mask alignment process where the x and y axes refer to the image plane, and the z axis refers to Δx. (a) Plot from a randomly misaligned mask. (b) Alignment about x and z axis corrected (alignment about x axis corrected by making step period at top and bottom of the mask constant, and about z axis by orientating steps vertically along z axis). (c and d) Rotation about y axis is progressively corrected, thus making the period of steps constant. (e) Plot is flattened by translating mask along z axis, leading to semi-optimal alignment (see text).

For each step in the procedure scans are performed by translating the mask along the x axis to generate the function G (Fig. 6), with ten translation steps typically used to generate the plot. At the start of the alignment procedure the position of the pixel edge is unknown so a scan of one period of the function, equal to the size of the pixel, is required. The following procedure is then repeated with the translation step size reduced on each iteration. For each iteration of the alignment procedure the range of the mask translation is centered around the best known position of the minimum of the detector response function. The plot of G is flattened, the translation step size then reduced with the procedure repeated until the desired resolution of mask alignment is achieved. A mask is said to be aligned to the precision of the translational increment when the plot of G appears flat. This procedure could easily be automated by using a minimization algorithm to flatten the plot of G.

Rotation about the x axis is optimized first, misalignment of this angle results in the steps in G appearing curved, as can be seen in Fig. 6a. This has the effect of creating a different number of steps in the plot of G for the top and bottom of the mask. An x axis rotation position is chosen where the number of steps in the function is equal for both the top and bottom areas of the mask, so that the steps appear straight. When this is the case both the top and bottom of the mask are at the same distance from the detector.

Next the mask is rotated about the z axis, which is coincident with the x-ray propagation direction as can be seen in the coordinate system shown in Fig. 1. The aim is to orient the steps vertically along the y axis of plot G, and when this is the case each transmission slit is parallel to a detector pixel column with steps oriented

vertically as shown in Fig. 6b.

Misalignment of rotation about the y axis changes the period of the steps over the function (Fig. 6b), as it effectively changes the distance of each slit along z from the detector. Rotation about the y axis is adjusted so that the period of the steps is constant, as shown in Fig. 6c and d.

Lastly the mask is translated along the z axis, which changes the distance between the steps in function G. As the mask approaches the correct position on z the distance between the steps gets larger (Fig. 6e), and when the mask is aligned these steps disappear. The translation step size is then reduced and the procedure repeated until the desired resolution of mask alignment is achieved.

The detector mask needs to be positioned so that the absorbing parts of the mask overlay the pixel edges, and the transmission slits overlay the center of the pixel columns. As a mask is aligned to the pixel edges this is achieved by translating the aligned detector mask along x by half the detector mask period, so leaving the detector mask in the correct position for imaging.

The sample mask can be aligned using the method described above, in which case no further steps need to be taken. The mask is only translated along the x axis to choose the correct illumination level for imaging.

B. Alignment of sample mask relative to detector mask

Using the method described previously for aligning the sample mask has the benefit that alignment is independent from any detector mask defects or small misalignment. Aligning the sample mask relative to the detector mask is though easier to perform as the signal to noise ratio is higher. This alternative method for aligning the sample mask is described as it gives a measure of the alignment of the whole system, and is used regularly to test for possible misalignment.

The procedure is essentially the same as that for a single mask, except now the detector mask replaces the detector response function. This means that the projected period of the sample mask is matched to the projected period of the detector mask, instead of the detector response function. A typical profile when translating the sample mask along x over the aligned detector mask is shown in Fig. 7. Equation 5 is modified so that a second mask replaces the detector response function (Eq. 10).

$$g(x, y; \Delta x) = I(x + \Delta x, y) \times T(x, y) \qquad (10)$$

As transmission slits of all current masks are less than half the mask period, the maximum of g (Eq. 10) is now found instead of the minimum, as this inflection point is sharper than the minimum (Eq. 11). The alignment procedure used is then exactly the same as outlined for single mask alignment, except Eq. 11 is now used instead of Eq. 6.
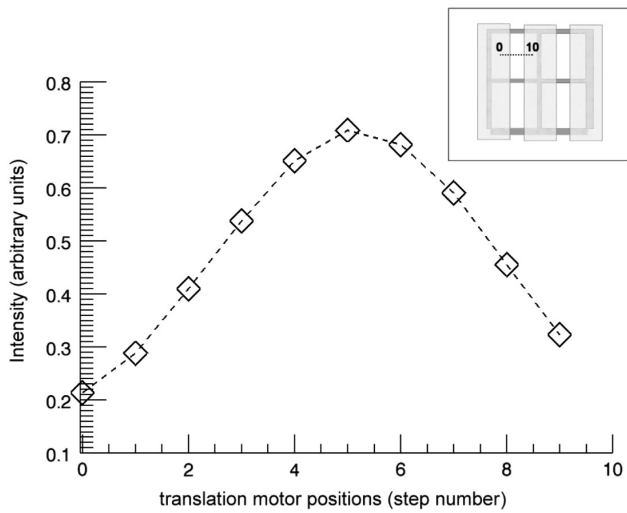
FIG. 7. Intensity detected in a single pixel when the aligned sample mask is scanned in the transverse x-direction in sub-pixel increments over the aligned detector mask.

$$G(x,y) = \max_{\Delta x} g(x,y;\Delta x) \qquad (11)$$

If this combined alignment procedure is run regularly then a record can be kept of any change of total system alignment over time. In practice though system alignment is stable; once aligned the system rarely needs any adjustment.

We currently operate a feedback mechanism whereby the detector output is used (jointly with the knowledge of the curve shown in Fig. 7) to keep the system dynamically aligned at the desired illumination level during long acquisitions (e.g. CT). The method described here would allow for a completely autonomous system as it could also allow for small adjustments to be made to alignment between imaging sequences.

VI. CONCLUSION

An alignment algorithm has been presented for an edge illumination XPCi system, that could be used to automate a future commercial system. This has been implemented using column-skipping and non-column-skipping laboratory systems, but could also be applied to a synchrotron based system. The algorithm can also be applied to either a single mask or two masks combined. Being able to measure the alignment of two masks combined means that the algorithm can be used to keep track of total system alignment over time. The algorithm then allows for automatic realignment, and for the continuation of imaging without manual intervention. As well

as being used for alignment the method also allows for a measure of any mask defects present. In practice this method has proved to be robust and reliable and is used to align all current system designs, and could be used for the automatization of future commercial systems.

[1] T. J. Davis, D. Gao, T. E. Gureyev, A. W. Stevenson, and S. W. Wilkins, Nature **373**, 595 (1995).
[2] R. A. Lewis, Physics in Medicine and Biology **49**, 3573 (2004).
[3] A. Snigirev, I. Snigireva, V. Kohn, S. Kuznetsov, and I. Schelokov, Review of Scientific Instruments **66**, 5486 (1995).
[4] V. N. Ingal and E. A. Beliaevskaya, Journal of Physics D: Applied Physics **28**, 2314 (1995).
[5] A. Momose, T. Takeda, Y. Itai, and K. Hirano, Nature medicine **2**, 473 (1996).
[6] S. W. Wilkins, T. E. Gureyev, D. Gao, A. Pogany, and A. W. Stevenson, Nature **384**, 335 (1996).
[7] D. J. Vine, D. M. Paganin, K. M. Pavlov, J. Krausslich, O. Wehrhan, I. Uschmann, and E. Forster, Applied Physics Letters **91**, 254110 (2007).
[8] I. Nesch, D. P. Fogarty, T. Tzvetkov, B. Reinhart, A. C. Walus, G. Khelashvili, C. Muehleman, and D. Chapman, Review of Scientific Instruments **80**, 093702 (2009).
[9] U. Bonse and M. Hart, Applied Physics Letters **6**, 155 (1965).
[10] C. David, B. Nohammer, H. H. Solak, and E. Ziegler, *Applied Physics Letters*, Applied Physics Letters **81**, 3287 (2002).
[11] A. Momose, Opt. Express **11**, 2303 (2003).
[12] T. Weitkamp, A. Diaz, C. David, F. Pfeiffer, M. Stampanoni, P. Cloetens, and E. Ziegler, Opt. Express **13**, 6296 (2005).
[13] F. Pfeiffer, T. Weitkamp, O. Bunk, and C. David, Nat Phys **2**, 258 (2006).
[14] A. Olivo, F. Arfelli, G. Cantatore, R. Longo, R. Menk, S. Pani, M. Prest, P. Poropat, L. Rigon, and G. Tromba, Medical physics **28**, 1610 (2001).
[15] A. Olivo and R. Speller, Applied Physics Letters **91**, 074106 (2007).
[16] A. Olivo and R. Speller, Phys Med Biol **52**, 6555 (2007).
[17] K. Ignatyev, P. R. T. Munro, D. Chana, R. D. Speller, and A. Olivo, Journal of Applied Physics **110**, 014906 (2011).
[18] A. Olivo, P. C. Diemoz, and A. Bravin, Opt. Lett. **37**, 915 (2012).
[19] P. R. Munro, K. Ignatyev, R. D. Speller, and A. Olivo, Proceedings of the National Academy of Sciences **109**, 13922 (2012).
[20] A. Olivo, S. E. Bohndiek, J. A. Griffiths, A. Konstantinidis, and R. D. Speller, Applied Physics Letters **94**, 044108 (2009).
[21] P. R. T. Munro, K. Ignatyev, R. D. Speller, and A. Olivo, Physics in Medicine and Biology **55**, 4169 (2010).
[22] J. C. Buckland-Wright, British Journal of Radiology **62**, 201 (1989).
[23] K. Ignatyev, P. R. T. Munro, R. D. Speller, and A. Olivo, Review of Scientific Instruments **82**, 073702 (2011).
[24] K. Ignatyev, A. Olivo, P. R. T. Munro, and R. D. Speller, "X-ray imaging," International Patent WO/2013/011316, 24/01/2013.
[25] W. Zhao and J. A. Rowlands, Medical Physics **22**, 1595 (1995).
[26] G. Pang, W. Zhao, and J. A. Rowlands, Medical Physics **25**, 1636 (1998).